Fluorine Depth Profiling Based on the 19F(p,p'g)19F Excitation Function

Joao Cruz (jdc@fct.unl.pt)
Universidade Nova de Lisboa Faculdade de Ciências e Tecnologia: Universidade Nova de Lisboa Faculdade de Ciencias e Tecnologia https://orcid.org/0000-0003-3242-0328

M. Fonseca
Universidade Nova de Lisboa FCT: Universidade Nova de Lisboa Faculdade de Ciencias e Tecnologia

D. Galaviz
Universidade de Lisboa Faculdade de Ciências: Universidade de Lisboa Faculdade de Ciencias

A. Henriques
LIP: Laboratorio de Instrumentacao e Fisica Experimental de Particulas

H. Luís
Instituto Tecnológico e Nuclear: Instituto Tecnologico e Nuclear

J. Machado
Universidade Nova de Lisboa FCT: Universidade Nova de Lisboa Faculdade de Ciencias e Tecnologia

P. Teubig
LIP: Laboratorio de Instrumentacao e Fisica Experimental de Particulas

P Velho
LIP: Laboratorio de Instrumentacao e Fisica Experimental de Particulas

V. Manteigas
Universidade Nova de Lisboa Faculdade de Ciencias e Tecnologia

A. P. Jesus
Universidade Nova de Lisboa Faculdade de Ciencias e Tecnologia

---

Research Article

Keywords: Ion beam analysis, geochemistry, archaeometry, PIGE (Particle Induced Gamma-ray Emission), ERYA-Profiling code.

Posted Date: September 16th, 2021

DOI: https://doi.org/10.21203/rs.3.rs-714711/v1

Fluorine Depth Profiling Based on the $^{19}F(p,p'\gamma)^{19}F$ Excitation Function

J. Cruz[1,2], M. Fonseca[1,2,3], D. Galaviz[4,5], A. Henriques[4], H. Luís[6], J. Machado[1,2], P. Teubig[4,5], P Velho[4], V. Manteigas[1], and A. P. Jesus[1,2]

1. Laboratório de Instrumentação, Engenharia Biomédica e Física da Radiação (LIBPhys-UNL)
2. Departamento de Física, Faculdade de Ciências e Tecnologia da Universidade Nova de Lisboa, Monte da Caparica, 2892-516 Caparica, Portugal
3. Lusófona University, HEI-Lab: Digital Human-Environment Interaction Lab, Lisbon, Portugal
4. Laboratório de Instrumentação e Física Experimental de Partículas, 1649-016 Lisboa, Portugal
5. Departamento de Física, Faculdade de Ciências da Universidade de Lisboa, Campo Grande, 1749-003 Lisboa, Portugal
6. Campus Tecnológico e Nuclear do Instituto Superior Técnico (CTN-IST), Estrada Nacional 10 (km 139,7), Bobadela, Loures, 2695-066 Bobadela LRS, Portugal

Abstract

Ion beam analysis of fluorine has applications in research on teeth and bones, materials science, geochemistry and archaeometry. A novel PIGE (Particle Induced Gamma-ray Emission) standard free methodology for fluorine content determination for in-depth heterogeneous samples based on the excitation function of the $^{19}F(p,p'\gamma)^{19}F$ nuclear reaction is presented. New precise cross section measurements of this reaction in the proton energy range 2.1 to 4.1 MeV have been performed. In addition, the ERYA-Profiling code, a computer program specially developed for PIGE analysis of in-depth heterogeneous samples, employed this new excitation function in a case study where different fluorine simulated depth profiles probed the capability of insight into fluorine distributions in a given sample, showing the potential of PIGE analysis.

Introduction

Fluorine is the most electronegative, reactive chemical element, and is also one of the most abundant in Earth's crust. Due to its chemical reactivity, it rarely occurs naturally in its elemental state; fluorine occurs in ionic forms (fluorides), or combined with other elements in minerals like fluorspar, fluorapatite, and cryolite.

Fluorine is highly toxic, but nonetheless it is widely used and forms an essential part of everyday life. Among other things, fluorides are used in the plastics industry (e.g., fluoropolymers and fluorine resins), and as additives to toothpaste and in LED bulbs to turn the cold LED light into a warm white. Fluorine compounds are also added to many pharmaceuticals to increase their effectiveness.

Over the years, the detection and characterization of fluorides, hydrogen fluoride, and fluorine has focused mainly on environmental and biological samples to understand and control the benefits and the potential toxicity that has been associated with fluorine uptake [1]. The standard detection method to analyze trace levels of fluorine in these samples are primarily the potentiometric (ion selective electrode, ISE) and gas chromatographic (GC) methods [2,3]. There are, nonetheless, other analytical tools available, such as inductively coupled plasma mass spectrometry (ICP-MS), atomic absorption spectrometry (AAS) and molecular absorption spectrometry (MAS) [4].

In the last years, the IAEA (International Atomic Energy Agency) has encouraged the development of PIGE (Particle Induced Gamma-ray Emission) as a standard technique in the quantification of elements lighter than sulfur [5]. PIGE, an IBA (Ion Beam Analysis) technique based on gamma-producing nuclear reactions, is particularly effective for fluorine detection and quantification in the outer few μm [6-13] due to the high sensitivity (below approx. 1 ppm) derived from high cross section values of the relevant nuclear reaction. Similar to PIXE (Particle Induced X-ray Emission), another ion-beam based analytical technique which already benefits from a wide use worldwide, PIGE demands small samples, does not destroy them, and provides multi-elemental information in a single spectrum.

Although complementary to PIXE in the sense that it covers light element analysis with the same kind of experimental facilities, PIGE, for a while, did not follow the same steps as PIXE towards a standard free technique based on the physical parameters which determine the radiation yield. On one side, the negligible absorption of radiation by the sample allows for

PIGE the use of standards in a straightforward reasonable approximation; on the other side, contrary to PIXE, nuclear reaction excitation functions are rarely smooth, displaying narrow and large resonances, which hindered the motivation to develop software for concentration calculations based on the cross sections.

In the last years, we have shown that, if cross sections are available in numerical values at energy steps close enough to define in detail the resonances, trivial integration leads to elemental concentrations for bulk samples [14-17]. Thus, these advances have allowed for the development of standard free PIGE methodology. The ERYA (Emitted Radiation Yield Analysis) code [15] was specifically developed to integrate the relevant nuclear reaction cross sections along the depth of homogeneous samples.

Resonances make PIGE a suitable technique for profiling fluorine in the outer few μm. In a review paper, Coote [18] presented a comprehensive list of depth profiling results using the PIGE technique for the surface analysis of inorganic materials (geochemistry, meteoritic material and man-made materials such as alloys) and organic materials (bone, teeth and fish scales). These studies relied on isolated strong and narrow resonances from the $^{19}F(p,p'\gamma)^{19}F$ and $^{19}F(p,\alpha\gamma)^{16}O$ nuclear reactions and they were selected according to the required yield, depth capability and depth resolution at the surface. These studies were limited to proton energies not higher than 1.5 MeV because above this value, resonances are much broader. This considerably limits the depth probed by PIGE. However, this limitation can be overcome by considering the whole excitation function which, in turn, requires a complete mathematical treatment and a computer code that implements it. Our group, continuing its work on ERYA, developed new a computer code, named ERYA-Profiling [19], that allows a full PIGE analysis of in-depth heterogeneous samples from resonance scanning profiling of the sample with an isolate resonance or more than one resonance, also including the direct component, as the contribution from the whole excitation function is calculated. Additionally, a non-homogeneous depth distribution of a given element may be inferred from the measured yield, taking advantage of broad features of the excitation function, as will be shown later.

Examples of pratical situations which benefit from this solution are: the study of fluorinated high-performance coatings, the investigation of layered structures in paintings and other pieces of art, the diffusion of fluorine into the teeth from surface applied treatments and the

uptake of fluorine from archeological bones. For such situations, where penetrating high energy beams may be required, insight into fluorine distribution in a given sample may be inferred from comparison between the calculated yield and corresponding measured gamma-ray yield at one or two different proton energies.

Naturally, a reliable output from ERYA-Profiling requires an accurate knowledge of nuclear reactions cross sections. For fluorine, the inelastic scattering reaction $^{19}F(p,p'\gamma)^{19}F$ is particularly relevant due to its high cross section values and to the fact that the main produced gamma-rays, 110 and 197 keV, are near the efficiency maximum of most gamma-ray detectors. From literature we conclude that the available experimental results are scarce, and results of different authors show large discrepancies up to a factor of two [20], especially above 2.5 MeV, which is an energy region of high interest. Although at a proton energy of 2.4 MeV a sensitivity of around 1 ppm may be reached [21], extending to higher energies up to around 4 MeV represents an upgrade as lower sensitivities may be obtained. Also, the sample may be probed at higher depths which may be relevant for in-depth heterogeneous samples.

To understand these discrepancies, a necessary step to give PIGE the role of a precise and reliable analytical technique, we present in this work results of new measurements of the gamma-producing cross sections of the $^{19}F(p,p'\gamma)^{19}F$ reaction for $\gamma_{1\text{-}0}$ = 110 keV and $\gamma_{2\text{-}0}$ = 197 keV, in the proton energy range 2.1 to 4.1 MeV. Compared to the existent data these measurements were done with a smaller energy step, allowing a better definition of the resonances. These precise new cross section values were implemented into the ERYA-Profiling to infer PIGE sensitivity to different simulated fluorine depth profiles.

PIGE methodology

Qualitatively, PIGE is based on the bombardment of solid samples by ions (typically protons with energies up to 4 MeV) which interact with sample nuclei, leading to a nuclear reaction with emission of gamma photons.

The gamma yield $dY(E,\theta)$ emitted by an isotope i, resulting from the interaction of N_p protons with energy E with a thin layer with areal density $N_i dx$ of the given isotope species is:

$$dY(E,\theta) = 4\pi\varepsilon_{abs}(E_\gamma)N_p\frac{d\sigma}{d\Omega}N_i dx \quad (1)$$

where N_i is the number of isotopes per volume unit, dx is the thin layer thickness, $\varepsilon_{abs}(E\gamma)$ is the absolute efficiency of the detector for γ rays with energy Eγ, and $d\sigma/d\Omega$ is the differential cross section for emission of a γ ray at angle θ with respect to the incident ion direction. For a thick sample, the beam with initial energy E_0 will steadily loose energy as it penetrates through the sample. The total gamma ray yield then becomes, assuming a constant mass fraction throughout the depth of the sample

$$Y(E_0,\theta) = 4\pi\varepsilon_{abs}(E_\gamma)N_p f_m f_i \frac{N_{av}}{A}\int_0^{E_0}\frac{1}{S_m(E)}\frac{d\sigma}{d\Omega}dE \qquad (2)$$

where $S_m(E)$ is the mass stopping power at energy E; f_m is the relevant element mass fraction; f_i, and A are the isotopic abundance and the atomic mass of the relevant element, respectively, and N_{av} is the Avogadro number. The factor $N_i/\rho = f_m f_i N_{av} A^{-1}$, where ρ is the mass density of the sample, transforms the atomic density into mass fraction also changing the linear stopping power to mass stopping power.

If the assumption of in-depth homogeneous samples is not valid, the gamma-ray yield, considering that the mass fraction may vary with depth, modifies to:

$$Y(E_0,\theta) = 4\pi\varepsilon_{abs}(E_\gamma)N_p f_i \frac{N_{av}}{A}\int_0^{E_0}\frac{f_m(E)}{S_m(E)}\frac{d\sigma}{d\Omega}dE \qquad (3)$$

If additionally, one considers that at a given depth, protons have an energy distribution $F_{\bar{E}}(E)$ with the mean proton energy equal to $\bar{E}$, the equation above turns into:

$$Y(E_0,\theta) = 4\pi\varepsilon_{abs}(E_\gamma)N_p f_i \frac{N_{av}}{A}\int_0^{E_0}\frac{f_m(\bar{E})}{S_m(\bar{E})}\left[\int_0^{\infty}F_{\bar{E}}(E)\frac{d\sigma}{d\Omega}dE\right]d\bar{E} \qquad (4)$$

Hence, Eq. (4) calculates the gamma-ray yields for samples with mass fraction varying with depth and takes into consideration the beam energy spread and the energy straggling within the sample.

So, to quantify the amount of fluorine from eq. (4), one requires the detector efficiency which depends on the energy of gamma-ray lines, the number of incident protons, i.e., the beam collected charge, the stopping powers corresponding to the main composition of the sample and finally the $^{19}F(p,p'\gamma_{1-0})^{19}F$ (Eγ = 110 keV) or the $^{19}F(p,p'\gamma_{2-0})^{19}F$ (Eγ = 197 keV) cross section values. To use eq. (4) the proton energy distribution along the depth of the sample must be included.

ERYA-Bulk [22], a recent version of ERYA, calculates gamma-ray yields for in-depth homogeneous samples from eq. (2), neglecting beam energy spread and energy straggling, since the effect of these on the bulk yield are negligible [23].

The ERYA-Profiling program, taking advantage of some functionalities and capabilities of ERYA-Bulk was developed for the analysis of in-depth heterogeneous samples from eq. (4), including a full treatment for straggling by using different energy distribution functions adequate to the amount of energy loss.

Experimental Procedure

The experimental work was carried out at the 3 MV Tandem accelerator of the Ion Beam Laboratory at CTN (Sacavém, Portugal) [24]. The proton beam, produced by a Duoplasmatron source is, after acceleration, deflected at a 90º analyzing magnet and a 25º switching magnet, passing through several focusing and steering electromagnetic devices before entering the target chamber. This configuration assured an energy resolution of 1 keV, measured by the 991 keV resonance of $^{27}Al(p,\gamma)^{28}Si$ reaction ($E\gamma = 1779$ keV, $\Gamma = 0.10$ keV). Beams with current intensities between 100 and 200 nA were used. The proton energy was calibrated with the 1645.1 and 1930.7 keV resonances of the reaction $^{23}Na(p,p'\gamma)^{23}Na$ and the 3470 keV resonance of the $^{16}O(p,p)^{16}O$ reaction.

At the entrance of the chamber, the beam passes through a collimator composed of a nickel foil with an aperture of 1 cm diameter and 2 mm of thickness, a gold foil with 1 mm thickness and an aperture of 2 mm and last a stainless-steal foil with the same dimensions as the gold one. These foils are mounted onto PVC structure and are electrically insulated from the chamber. To assure a good reproducibility of beam charge collection, the chamber is insulated from the beam line and pumping system, to act together with the target holder and beam stopper as one Faraday cage.

Gamma-ray detection was accomplished by a 45% relative efficiency HPGe detector having a nominal resolution of 2.2 keV for the 1173 keV ^{60}Co gamma-line, placed at an angle of 130º to the beam direction. The detector absolute efficiency was determined by means of radioactive sources of ^{133}Ba and ^{152}Eu (with several energy lines between 81 keV and 1.5 MeV), calibrated in activity with an uncertainty of 5%, placed at the target position.

Besides the gamma-ray detector, a PIPS detector, placed at an angle of 160º to the beam axis was used in this experiment to collect backscattered particles from the target. With an intrinsic efficiency of 100 % and a resolution of 15 keV for 5 MeV alpha particles, its solid angle was determined with 2 % uncertainty by measuring with high accuracy the diameter of the aperture placed in front of the detector and the distance between the target and the detector.

The target was prepared by vacuum evaporating a thin sodium fluoride layer on a previously evaporated silver self-supporting film.

Results

Cross Section Measurement

To avoid the uncertainties associated to the measurement of the absolute number of incident protons (beam charge collection) and of the target thickness, it was measured simultaneously the Rutherford backscattering yield of a heavy component of the target i.e., the Ag self-supporting film.

For thin targets as the one used in this work, and at off resonance or on resonances that are large when compared with the target energy thickness, the radiation yield, collected within a small solid angle, is given directly by eq.(1), with d$Y(E,\theta) \approx Y(E,\theta)$, becoming:

$$Y(E,\theta) = 4\pi\varepsilon_{abs}(E_\gamma)N_p\frac{d\sigma}{d\Omega}n_F \qquad (5)$$

where n_F is the number of fluorine nuclei in the target per surface unit, and the other quantities have been defined previously.

The number of protons elastically scattered by silver at an angle β, inside a small solid angle, may be determined by:

$$Y_p^{Ag} = \varepsilon_p\Omega_p N_p\left(\frac{d\sigma}{d\Omega}\right)_{Ruth}^{Ag} n_{Ag} \qquad (6)$$

where N_p is the number of incident protons with energy E, n_{Ag} is the number of silver nuclei in the target per surface unit, Ω_p and ε_p are respectively the solid angle and the intrinsic efficiency of the particle detector and $\left(\frac{d\sigma}{d\Omega}\right)_{Ruth}^{Ag}$ is the proton Rutherford backscattering cross-section on silver, which can be calculated analytically.

From the two previous equations, the differential cross-sections for the 110 keV and 197 keV gamma-rays were calculated using:

$$\frac{d\sigma}{d\Omega} = \frac{Y(E,\theta)}{Y_p^{Ag}}\, r\, \frac{\varepsilon_p \Omega_p}{4\pi\, \varepsilon_{abs}(E_\gamma)} \left(\frac{d\sigma}{d\Omega}\right)_{Ruth}^{Ag} \qquad (7)$$

where r is a stoichiometric factor which represents the relation between the density of atoms of silver and fluorine in the target ($r = n_{Ag}/n_F$) and has been obtained by alpha particle RBS (Rutherford Backscattering Spectrometry) analysis of the sample: $n_F = 5.0\times10^{17}$ at./cm^2 and $n_{Ag} = 3.2\times10^{17}$ at./cm^2. The Ag Rutherford cross section was calculated neglecting the beam energy loss at the sodium fluoride layer, which amounts to a 0.6% variation at 2.1 MeV beam energy and 0.2% at 4.1 MeV.

The cross-section uncertainties are listed in table 1, where a separation between statistical and systematic uncertainties is made.

Table 1. Uncertainty budget for the measurements

Statistical uncertainties	
γ-ray peak area (statistics and area determination)	2%
Proton (Ag) peak area (statistics and area determination)	1%
Ruth. cross section (beam energy resolution = 1 keV)	< 0.1%
Overall relative uncertainty	2.3%
Systematic uncertainties	
γ-ray detector efficiency	7%
Proton detector solid angle	2%
Ratio of F to Ag	3%
Overall absolute uncertainty	7.9%

To keep the systematic uncertainties under control, the target stability, the beam charge collection, the detection system, and the background contributions to the gamma lines were monitored throughout the whole measurement. The choice of materials for the entrance collimator ensured that all detected 110 and 197 keV photons were coming from the target. Measurements were repeated at several energy points to ensure that experimental conditions

were kept unchanged and to check target stability under proton bombardment. In the described conditions, systematic uncertainties affect only the overall scale of cross section values.

Fig. 1 shows a gamma spectrum obtained at 2464 keV proton energy, where the 110 keV and 197 keV lines are clearly separated from other gamma lines. The corresponding scattered proton spectrum is presented in fig. 2, showing that the peak relative to Ag is also separated from the other peaks, which are identified in the figure.

Excitation functions for the $^{19}F(p,p'\gamma)^{19}F$ reaction are presented in red in Fig. 3 for the 110 keV line and in fig. 4 for the 197 keV line. Numerical values are available in the IBANDL database for PIGE [20].

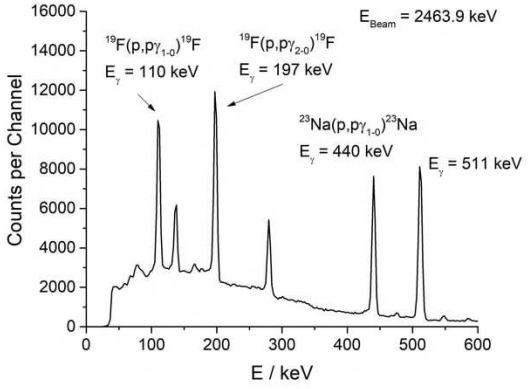

Fig. 1 Gamma-ray spectrum obtained at 2464 keV proton energy clearly showing the gamma-ray lines to be quantified.

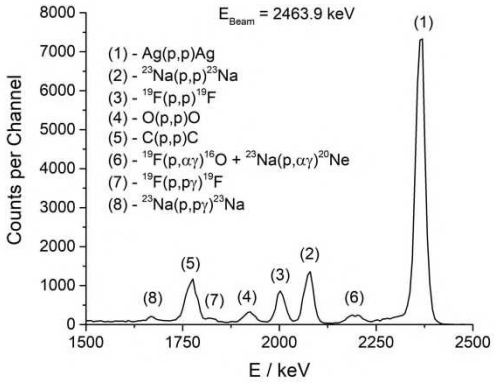

Fig. 2 Scattered proton spectrum obtained at 2464 keV proton energy showing the Ag peak separated from the other peaks.

Comparison of our results with the ones available in IBANDL database for PIGE [5, 25-30] are shown in fig. 3 for the 110 keV line and in fig. 4 for the 197 keV line. Despite the proton energy deviation from 5 to 10 keV among different authors, off resonance or in broad resonances, a quantitative comparison among authors may be done.

In relation to the 110 keV gamma-ray line, the results of the other authors are in fair agreement below 2.8 MeV, but above this energy C. Boni [30] and W.A. Ranken [25] results

are around 50% higher than the other values. This work brings validation to the lower values, agreeing with them within the experimental uncertainty.

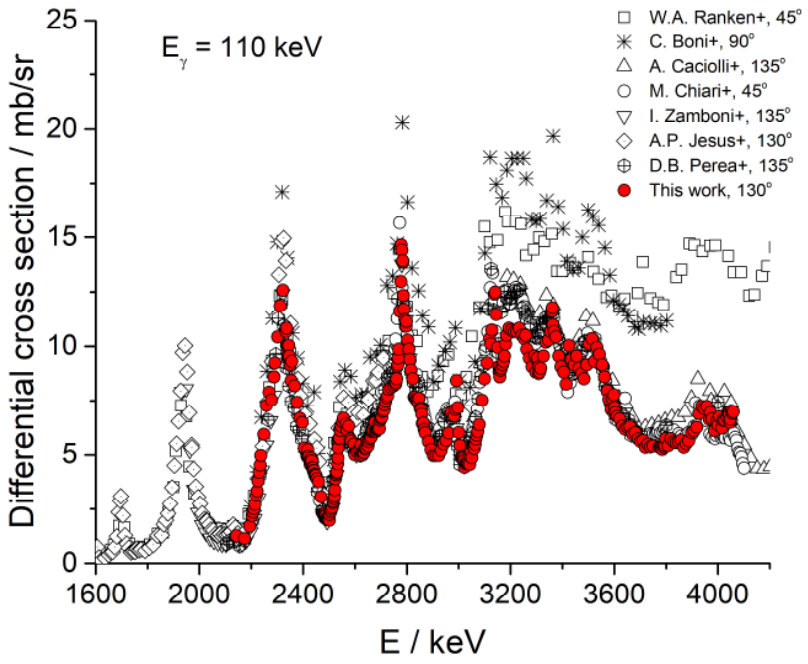

Fig. 3 Comparison of the results concerning the cross sections of the reaction $^{19}F(p,p'\gamma_{1-0})^{19}F$ measured in this work with those measured by other authors [5, 25-30].

For the 197 keV gamma line, there is a larger scatter of values of previously published results. In the first large resonance results of A.P. Jesus [29] and D.B. Perea [26] are in close agreement, but lower by 30% in relation to values of I. Zamboni [28] and C. Boni [30]. In the second and third resonances the discrepancy of the values of these authors relative to A.P. Jesus [29] and D.B. Perea [26] increase, and values of M. Chiari [5] are still higher, reaching a factor close to two, trend that is kept through the whole energy range. Above 3 MeV there is a fair agreement between values obtained by A. Caccioli [27], W.A. Ranken [25] and D.B. Perea [26], but results of C. Boni [30] and M. Chiari [5] are almost a factor of two larger than those. Again, the values obtained in this work confirm the trend of lower cross sections, for the whole energy range. For authors displaying lower values of the cross sections (previous works and this work), the respective results are generally within the uncertainties in relation to the average.

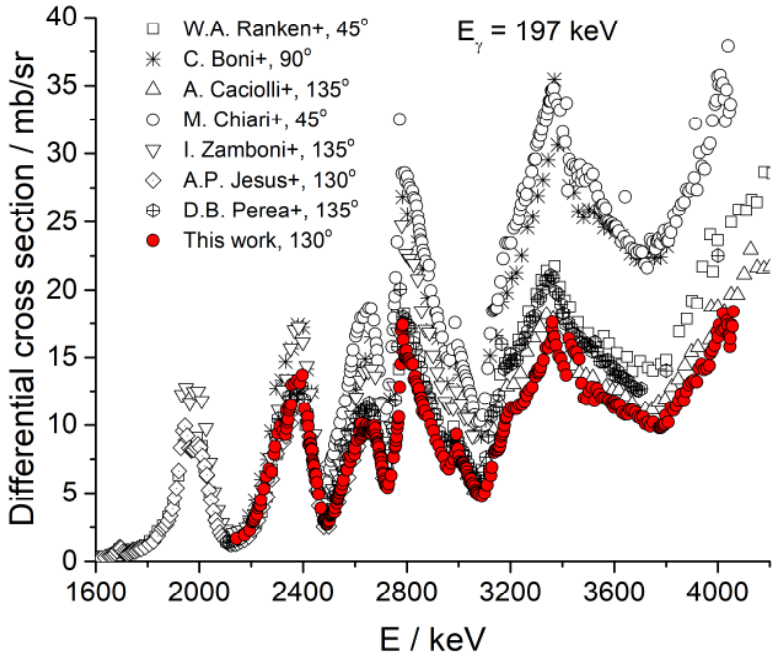

Fig. 4 Comparison of the results concerning the cross sections of the reaction $^{19}F(p,p'\gamma_{2-0})^{19}F$ measured in this work with those measured by other authors [5, 25-30].

Although the 110 keV line, originating at a j=1/2 level is expected to be isotropic, the same does not apply to the 197 keV line coming from a j=5/2 level. However, all the measurements were done at similar or equivalent angles, 130°, 135° and 45°, except for C. Boni [30] who measured at 90°.

Hence, for both gamma lines, the results obtained in this work give weight to a statistical rejection of C. Boni [30] and M. Chiari [5] values for the 197 keV line and C. Boni [30] and W.A. Ranken [25] (above 3.1 MeV) values for the 110 keV line.

Fluorine depth profiling with ERYA-Profiling

With the ERYA-Profiling database updated with the new $^{19}F(p,p'\gamma_{2-0})^{19}F$ (E_γ = 197 keV) excitation function, an hypothetical case study, fluorine in silicon substrate, is presented to illustrate PIGE depth resolution sensitivity when the whole excitation function is considered.

Technologically, fluorine in silicon has been studied to determine surface contaminants of silicon wafers after procedures such as etching and polishing or to investigate implanted silicon samples ([18] and references therein). Three different depth distributions with the same total amount of fluorine, in a silicon thick sample, were defined considering in ERYA-Profiling five layers, each with a fixed amount of fluorine and silicon (Table 2). In fig. 5 the fluorine concentration per layer is represented as function of the proton energy, as a conversion from depth in at./cm^2 was made to proton energy, taking into consideration the energy thickness of each layer and the energy loss of the beam along the sample. The distributions are: a gaussian-like shape (red line), an exponential-like shape (blue line), and a see-saw shape (green line). These distributions were chosen to simulate a gaussian implanted profile (true for low fluence implantations), diffusion from the surface and a layered structure, respectively. In fig. 5 a) the layers correspond to 2.7×10^{19} at./cm^2 of Si per layer, i.e., 5.5 μm total thickness, and a total of 5.0×10^{18} at./cm^2 of F. In fig. 5 b) the layers correspond to 5.4×10^{18} at./cm^2 of Si per layer, i.e., 1.1 μm total thickness, and a total of 5.0×10^{17} at./cm^2 of F (so chosen to be of the same magnitude relative to Si as in the previous situation). Detailed information on F amounts per layer for the different distributions are given in table 2. A fourth configuration is also shown in fig. 5 (yellow line), corresponding to a in-depth homogeneous distribution of F (same total amount) in Si throughout the range of protons in Si.

In fig. 5 the excitation function corresponding to the 197 keV gamma-ray line is also shown allowing the perception that different parts of the 197 keV gamma-ray excitation function contribute to the gamma yield coming from fluorine. As the gamma yield is mostly proportional to the product of the cross section by the fluorine atomic concentration, a quick inspection of fig. 5 a) is enough to understand that different yields will be obtained for the different distributions. Gamma yield values correspondent to the three distributions were calculated by ERYA-Profiling and displayed in table 2, confirming a clear distinction among the distributions. Yields refer to 3350 keV proton energy, our detection efficiency (= 0.0181) and 1.0 μC of collected charge.

It is true that one distribution with one given fluorine total amount and another distribution with a different fluorine total amount may lead to the same value of the gamma yield. However, note that if the yields are the same at a given incident energy, they will differ at

another energy and also differ for the 110 keV gamma-line whose excitation function differs from the one corresponding to the 197 keV line (see figures 3 and 4).

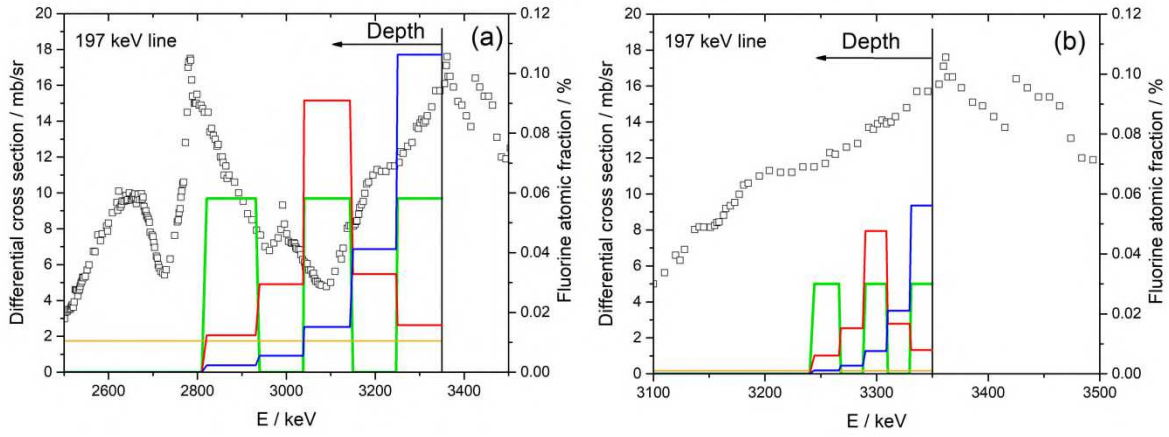

Fig 5. Different in-depth distributions, with the same total amount of fluorine in silicon: gaussian-like shape (red line), exponential-like shape (blue line), and see-saw shape (green line). The yellow line, corresponds to a in-depth homogeneous distribution of F in Si throughout the range of 3350 keV protons in Si. The excitation function corresponding to the 197 keV gamma-ray line, coming from the inelastic scattering of protons by fluorine, is also shown in both figures. In fig. 5 a) the layers correspond to 2.7×10^{19} at./cm^2 of Si per layer, and a total of 5.0×10^{18} at./cm^2 of F. In fig. 5 b) the layers correspond to 5.4×10^{18} at./cm^2 of Si per layer, and a total of 5.0×10^{17} at./cm^2 of F.

Analyzing situations with narrower and narrower distributions of fluorine lead to the situation illustrated in fig. 5 b), where only a small part of the excitation function is responsible for the gamma-ray yield. This translates into a lower capacity of distinction, which in this case, and for 3350 keV proton energy, means yields that differ from each other by 10%, slightly higher than the experimental uncertainty of measured yields. This gives a perspective of the depth resolution (~1 μm for Si) that may be reached at this energy. However, moving to a lower portion of the excitation function with closer resonances and a steeper gradient of cross section per energy, this may be improved. Considering the proton incident energy of 2800 keV, one obtains for the Gaussian like, see-saw like, exponential like and homogeneous configurations yields respectively equal to 5811, 7245, 9560 and 2545. Notice that now the three first configurations differ by more than 25%.

Table 2. Layer amounts of F for three different in-depth distributions and correspondent calculated gamma-ray yields for the 197 keV line, coming from the inelastic scattering of protons by ^{19}F. For each case, the distributions have the same total amount of fluorine in silicon (thick sample). Si and F amounts are given in units of 10^{15} at./cm^2. Layers are numbered 1 to 5 starting from the surface of the sample, which is bombarded by protons with an energy of 3350 keV. The yields are calculated by ERYA-Profiling for our detection system and 1μC of collected charge. For comparison, the gamma-ray yield, corresponding to the same amount of fluorine with a homogeneous distribution throughout the range of 3350 keV protons in Si, is also given.

	Fig. 5 (a): in each layer 2.7×10^4 of Si; total amount of F: 5×10^3					Calculated
Distributions	Layer 1	Layer 2	Layer 3	Layer 4	Layer 5	γ yield
Gaussian-like	400	850	2500	850	400	54844
Sea-saw-like	1670	0	1670	0	1660	113424
Exponential	3210	1160	415	149	66	85004
Homogeneous	Throughout the range of 3350 keV protons in Si					36249
	Fig. 5 (b): in each layer 5.4×10^3 of Si; total amount of F: 5×10^2					Calculated
Distributions	Layer 1	Layer 2	Layer 3	Layer 4	Layer 5	γ yield
Gaussian-like	40	85	250	85	40	9499
Sea-saw-like	167	0	167	0	166	10487
Exponential	321	116	41.5	14.9	6.6	11076
Homogeneous	Throughout the range of 3350 keV protons in Si					3625

Discussion

What are the implications of the excitation functions and their uncertainties and discrepancies for fluorine bulk and profiling analysis? An overall deviation factor in the cross sections translates (see eq. 2 and 4) directly in the same deviation of the corresponding calculated yield or mass fraction of the element. Also, the combined uncertainty of cross section values, of the absolute value of the collected carge, of the detector efficiency and of the stopping powers leads to an uncertainty of the determined mass fractions which may be larger than 20%, considering the quoted uncertainites of a given excitation function.

However, this may be improved if calibrations are performed (as it is also done for standard-less PIXE). For each light element to be analysed, the gamma-ray yield of a pellet made of pure inorganic compound containing the element or of a standard reference sample must be measured and compared with the corresponding calculated yield. The ratio of the experimental and calculated yield will then be used as an external calibration factor (or correction factor) in future analysis of that element, provided the same experimental conditions (e.g. ion beam, detector type and detector geometry) are used and also the same excitation function for the calculations. In order to confirm the stability of experimental

conditions (mainly of the charge measurement), one might use a lithium or boron standard sample (the cross sections related to $^{7}Li(p,p'\gamma)^{7}Li$ and $^{10}B(p,\alpha\gamma)^{10}B$ reactions are smooth) and measure its yield before each analytical running time. An uncertainty around 5% which is the uncertainty of stopping power values is then attainable.

Notice that, compared to the true excitation function, one given experimental excitation function may exhibit deviations that are not constant within the whole energy range. We have seen it in the comparison shown before (fig. 3 and 4). This implies that a calibration factor measured at a given energy may not be valid at another energy. Also, it is evident from the hypothetical case that absolute uncertainties will directly affect the values of fluorine amounts, and the relative uncertainties (portions of the excitation function versus another) will influence the distributions.

Hence, it is important to rely on a detailed and precise excitation function measurement (such as ours) where in relative terms (one energy range versus another) conditions were assured to keep constant any quantities leading to systhematic uncertainties.

Conclusions

The excitation functions of $^{19}F(p,p'\gamma)^{19}F$ reaction for $\gamma_{1\text{-}0}$ = 110 keV and $\gamma_{2\text{-}0}$ = 197 keV, in the proton energy range 2.1 to 4.1 MeV were obtained in this work, with a careful experimental procedure to assure low absolute (in terms of the cross section values scale) and relative (among different points and portions of the excitation function) uncertainties. This experiment also brought in comparison to previous existing data a more detailed knowledge and resonance definition.

The capacity gained with an application (ERYA-Profiling) to deal with in-depth heterogeneous samples employing the whole excitation function was presented. Insight into fluorine distributions down to a depth resolution below 1 μm was demonstrated. This allows to handle specific problems where high energy beams to go deeper into the sample are required.

Acknowledgments

The authors acknowledge LIBPhys (UID/FIS/04559/2019) and NOVA.ID.FCT.

Data availability

Data are available on request from the authors.

Competing interests: The authors declare no competing interests.

References

[1] Nichole R. Johnston, Scott A. Strobel, Arch. Toxicol. 94, 1051–1069 (2020) https://doi.org/10.1007/s00204-020-02687-5

[2] Toxicological profile for fluorides, hydrogen fluoride and fluorine (U.S. Department of Health and Human Services, 2003), https://www.atsdr.cdc.gov/toxprofiles/tp11-p.pdf. Accessed 6 July 2021

[3] R. Fuge, Appl. Geochem. 100, 393-406 (2019). https://doi.org/10.1016/j.apgeochem.2018.12.016

[4] A. Dhillon, M. Nairb, D. Kumar, Anal. Methods, 2016,8, 5338-5352 (2016). https://doi.org/10.1039/C6AY01534D

[5] Development of a Reference Database for Particle Induced Gamma Ray Emission (PIGE) Spectroscopy (IAEA-TECDOC-1822, Vienna, 2017) https://www.iaea.org/publications/12235/development-of-a-reference-database-for-particle-induced-gamma-ray-emission-pige-spectroscopy. Accessed 6 July 2021

[6] M.Döbeli, A.A.-M.Gaschen, U.Krähenbühl, in Advances in Fluorine Science vol.2, ed. by A. Tressaud (Elsevier, Netherlands, 2006), p. 215

[7] C. S. Sastri, A. Banerjee, T. Sauvage, T. et al., J. Radioanal. Nucl. Ch. 298, 311–315 (2013). https://doi.org/10.1007/s10967-012-2410-x

[8] D.D. Cohen, E. Stelcer, O. Hawas, D. Garton, Nucl. Instrum. Meth. B 219–220, 145-152 (2004). https://doi.org/10.1016/j.nimb.2004.01.043

[9] R. Mateus, M.A. Reis, A.P. Jesus and J.P. Ribeiro, Nucl. Instrum. Meth. B 249, 784-788 (2006). https://doi.org/10.1016/j.nimb.2006.03.139

[10] P.S. Dhorge, R. Acharya, N. S. Rajurkar, V. Chahar, V. Tuli, A. Srivastava, P. K. Pujari, J. Radioanal. Nucl. Ch. 311, 1803–1809 (2017) https://link.springer.com/article/10.1007/s10967-016-5118-5

[11] F. Lucarelli, G. Calzolai, M. Chiari, S. Nava, L. Carraresi, Nucl. Instrum. Meth. B 417, 121-127 (2018). https://doi.org/10.1016/j.nimb.2017.07.034

[12] F. Lucarelli, Eur. Phys. J. Plus 135, 538 (2020). https://doi.org/10.1140/epjp/s13360-020-00516-3

[13] C. Heckel, K. Müller, R. White, S. Wolf, N.J. Conard, C. Normand, H. Floss, I. Reiche, Quaternary International 403, 40-50 (2016). https://doi.org/10.1016/j.quaint.2015.11.105.

[14] R. Mateus, A.P. Jesus, J.P. Ribeiro (2004), Nuclear Instruments and Methods B 219-220, 519-523, https://doi.org/10.1016/j.nimb.2004.01.114

[15] R. Mateus, A. P. Jesus, J. P. Ribeiro, Nucl. Instrum. Meth. B 229, 302-308 (2005) https://doi.org/10.1016/j.nimb.2004.11.019

[16] R. Mateus, M. Fonseca, A.P. Jesus, H. Luís, J.P. Ribeiro, Nucl. Instrum. Meth. B 266, 1490-1492 (2008). https://doi.org/10.1016/j.nimb.2007.11.042

[17] M. Fonseca, A. P. Jesus, H. Luís, R. Mateus, J. Cruz, L. Gasques, D. Galaviz, J. P.

Ribeiro, Nucl. Instrum. Meth. B 268, 1806-1808 (2010). https://doi.org/10.1016/j.nimb.2010.02.079

[18] G.E. Coote, Nucl. Instrum. Meth. B 66, 191-204 (1992)

[19] V. Manteigas, J. Cruz, M. Fonseca, A.P. Jesus, Nucl. Instrum. Meth. B 502 (2021) 142-149, https://doi.org/10.1016/j.nimb.2021.06.006

[20] IAEA Ion Beam Analysis Nuclear Data Library (IBANDL), https://www-nds.iaea.org/exfor/ibandl.htm

[21] R. Mateus, A.P. Jesus, M. Fonseca, H. Luís, J.P. Ribeiro, Nucl. Instrum. Meth. B 264, 340-344 (2007). https://doi.org/10.1016/j.nimb.2007.09.030

[22] ERYA-Bulk webpage. https://sites.fct.unl.pt/nuclear/software/erya-bulk . Accessed 6 July 2021

[23] N. Pessoa Barradas, J. Cruz, M. Fonseca, A.P. de Jesus, A. Lagoyannis, V. Manteigas, M. Mayer, K. Preketes-Sigalas, P. Dimitriou, Nucl. Instrum. Meth. B 468, 37-47 (2020). https://doi.org/10.1016/j.nimb.2020.02.019

[24] E. Alves, K. Lorenz, N. Catarino, M. Peres, M. Dias, R. Mateus, L.C. Alves, V. Corregidor, N. P. Barradas, M. Fonseca, J. Cruz, A. Jesus, Eur. Phys. J. Plus 136, 684 (2021). https://doi.org/10.1140/epjp/s13360-021-01629-z

[25] W. A. Ranken, T. W. Bonner, and J. H. McCrary, Phys. Rev. 109, 1646 (1958). https://doi.org/10.1103/PhysRev.109.1646

[26] D. Bachiller Perea, P. Corvisiero, D. Jiménez Rey, V. Joco, A. Maira Vidal, A. Muñoz Martin, A. Zucchiatti, Nucl. Instrum. Meth. B 406, 161-166 (2017). https://doi.org/10.1016/j.nimb.2017.02.017

[27] A. Caciolli, M.Chiari, A. Climent-Font, M.T. Fernández-Jiménez, G. García-López, F. Lucarelli, S. Nava, A. Zucchiatti, Nucl. Instrum. Meth. B 249, 98-100 (2006). https://doi.org/10.1016/j.nimb.2006.03.089

[28] I. Zamboni, Z. Siketic, M. Jakšic, I. Bogdanovic Radovic, Nucl. Instrum. Meth. B 342 266-270 (2015). http://dx.doi.org/10.1016/j.nimb.2014.10.022

[29] A.P. Jesus, B. Braizinha and J.P. Ribeiro, Nucl. Instrum. Meth. B 161-163, 186-190 (2000). https://doi.org/10.1016/S0168-583X(99)00855-1

[30] C. Boni, E. Cereda, G.M. Braga Marcassan and V. de Tomasi, Nucl. Instrum. Meth. B 35, 80–86 (1988)